Research Square

Preprints are preliminary reports that have not undergone peer review.
They should not be considered conclusive, used to inform clinical practice,
or referenced by the media as validated information.

Morphological Variations of the Infraorbital Foramen and Canal: A Cross-Sectional Analysis Using Cone Beam Computed Tomography (CBCT) in an Iranian Population

Shirin Sakhdari
Islamic Azad University Dental Branch of Tehran
Amirhossein Aref
Islamic Azad University Dental Branch of Tehran
Abolfazl Azimi
azimiabolfazl80@gmail.com

Islamic Azad University Dental Branch of Tehran

Research Article

Keywords: Anatomy, Cross-Sectional, Cone-Beam Computed Tomography, Maxillary Nerve, Maxillary Sinus

Posted Date: November 13th, 2026

DOI: https://doi.org/10.21203/rs.3.rs-11568795/v1

License: This work is licensed under a Creative Commons Attribution 4.0 International License.
Read Full License

Additional Declarations: No competing interests reported.

Morphological Variations of the Infraorbital Foramen and Canal: A Cross-Sectional Analysis Using Cone Beam Computed Tomography (CBCT) in an Iranian Population

Authors:

Shirin Sakhdari[1], Amirhossein Aref[1], Abolfazl Azimi[1]*

Affiliations:

[1] Department of Oral and Maxillofacial Radiology, Tehran Medical Sciences, Islamic Azad University, Tehran, Iran

Corresponding Author:

Abolfazl Azimi, DDS

Department of Oral and Maxillofacial Radiology

Faculty of Dentistry, Tehran Medical Sciences

Islamic Azad University

Tehran, Iran

E-mail: azimiabolfazl80@gmail.com

ORCID iDs:

- Shirin Sakhdari: https://orcid.org/0000-0003-1686-5538
- Abolfazl Azimi: https://orcid.org/0009-0009-3631-083X

Abstract

Purpose: The infraorbital nerve's anatomical variations relative to the maxillary sinus pose risks during maxillofacial surgeries, potentially leading to iatrogenic injuries like paresthesia or hemorrhage. Precise morphometric knowledge via cone-beam computed tomography (CBCT) is essential for preoperative planning, yet data in Iranian populations remain limited.

Methods: This retrospective cross-sectional study analyzed 128 CBCT images (256 sides) from patients (64 males, 64 females; mean age 30.45 ± 12.6 years) referred to a dental school and private radiology center. Infraorbital canal (IOC) types were classified as: Type 1 (embedded in sinus roof), Type 2 (partial protrusion), Type 3 (full protrusion), Type 4 (lateroantral). Infraorbital foramen (IOF) shapes were categorized as oval, triangular, or semilunar/circular. Data on gender, age (<30/≥30 years), side, and symmetry were assessed using chi-square tests ($P < 0.05$).

Results: Oval IOF predominated (85.1%), with no gender (P=0.351), side (P=0.953), or age (P=0.907) differences; symmetry was 88.3%. IOC Type 1 was most common (57.4%), followed by Type 2 (28.9%), Type 4 (9.8%), and Type 3 (3.9%), with no overall gender (P=0.867), side (P=0.997), or age (P=0.980) variations, though Type 1 predominated within genders (females: P=0.0046; males: P=0.0013). IOC symmetry was 74.2% (Type 1: 47.7%, P<0.0001).

Conclusion: Morphological variations in IOF and IOC exhibit high symmetry and gender-specific patterns, emphasizing CBCT's role in mitigating surgical risks.

Keywords: *Anatomy, Cross-Sectional; Cone-Beam Computed Tomography; Maxillary Nerve; Maxillary Sinus*

Introduction

The infraorbital nerve (ION), a major terminal branch of the maxillary division (V2) of the trigeminal nerve, originates from the pterygopalatine fossa and courses anteriorly through the infraorbital groove (IOG) on the orbital floor before entering the infraorbital canal (IOC) and exiting via the infraorbital foramen (IOF) approximately 6-10 mm inferior to the infraorbital rim. This nerve provides sensory innervation to the lower eyelid, lateral nose, upper lip, maxillary gingiva, and anterior maxillary teeth, making it a critical structure in the maxillofacial region (1). Anatomical variations in the IOC and IOF are well-documented, with recent systematic reviews classifying IOC configurations into four types based on their relationship to the maxillary sinus (MS): Type 1 (contained within or below the MS roof), Type 2 (partially protruding into the MS), Type 3 (fully protruding or suspended into the MS lumen), and Type 4

(located laterally in the orbital floor or zygomatic recess) (1, 2). In Iranian populations, recent CBCT analyses have shown the IOF-midline distance to be significantly greater in males (mean 26.5 mm) than females (mean 24.8 mm), highlighting the need for region-specific data to inform clinical practice (3).

The proximity of the ION to the MS and orbital floor poses substantial risks during maxillofacial surgeries, such as endoscopic sinus surgery, Le Fort I osteotomies, orbital reconstructions, and sinus lifts, where iatrogenic injury can result in sensory disturbances like paresthesia, hypoesthesia, or chronic neuropathic pain in up to 12-27% of cases, particularly with Type 3 IOC protrusions (1, 4, 5). Recent studies emphasize that unrecognized IOC protrusions increase the likelihood of nerve transection or compression, leading to complications including hemorrhage, orbital hematoma, or prolonged recovery, with higher incidences in the presence of Haller cells or MS septa (6). Traditional two-dimensional imaging, such as panoramic radiography, is limited by superimposition, magnification errors (up to 25%), and poor resolution of three-dimensional structures, often failing to accurately depict IOC variants or MS relationships, which can lead to intraoperative surprises (7, 8). In contrast, cone-beam computed tomography (CBCT) provides multiplanar reconstructions with submillimeter isotropic resolution (0.075-0.4 mm), lower radiation doses (20-200 μSv vs. 500-1000 μSv for medical CT), and superior visualization of bony anatomy, enabling precise morphometric analysis of the IOF and IOC without distortion (9, 10).

Despite advances in CBCT-based research, studies on IOC and IOF morphology in Middle Eastern populations, particularly Iranians, remain limited, with earlier investigations showing Type 1 IOC predominance (57-68%) but lacking comprehensive symmetry and age-stratified analyses (3, 11). This gap is critical, as ethnic variations influence surgical outcomes, and no recent large-scale Iranian cohort has fully explored gender, age, and bilateral symmetry factors (1, 12). The present study aimed to evaluate morphological variations of the IOF (oval, triangular (13), semilunar/circular) and IOC (Types 1-4) using CBCT images from 128 Iranian patients alongside associated factors like age, gender, side, and symmetry. Hypotheses tested were: (1) equivalent prevalence of morphological types across age groups; (2) equivalent prevalence across genders; and (3) general asymmetry in IOF and IOC types between sides.

Materials and Methods

Study Design

This retrospective analytical cross-sectional study was designed to evaluate the morphological variations of the infraorbital foramen (IOF) and infraorbital canal (IOC) using cone-beam computed tomography (CBCT) images. The research adhered to the Strengthening the Reporting of Observational Studies in Epidemiology (STROBE) guidelines for cross-sectional studies to ensure comprehensive and transparent reporting. All procedures were conducted in accordance with ethical standards, and the study protocol was

reviewed and approved by the Institutional Review Board of a dental school (approval number IR.IAU.DENTAL.REC.1399.306 for retrospective image analysis, as per institutional policy for anonymized data).

Participants

A total of 128 CBCT images were selected from patients referred to the Radiology Department of a dental school and private maxillofacial radiology center in Tehran, Iran, between March 2020 and March 2021. The sample comprised 64 males and 64 females, with a mean age of 30.45 years (standard deviation [SD] 12.6 years; range 14-77 years). Inclusion criteria required CBCT scans that fully encompassed the maxillary sinus and at least the inferior third of the orbital cavity bilaterally, ensuring adequate visualization of the IOC and IOF. Exclusion criteria were applied to minimize confounding factors and included: evidence of maxillary or orbital trauma; prior surgery in the maxillary sinus; pathological changes such as cysts, tumors, or infections in the maxillary sinus; congenital or acquired maxillary sinus anomalies; orbital fractures; edentulism in the maxillary arch; and presence of impacted or congenitally missing canines, as these could alter anatomical landmarks or canal morphology.

Sample size calculation was performed a priori using G*Power software (version 3.1.9.7) based on morphometric data from a previous study by Acar et al. (2018) (6). Assuming an effect size of 0.5 for subgroup comparisons, a standard deviation of 2.7 mm for canal measurements, an alpha error probability of 0.05, and a statistical power of 80%, a minimum of 64 images per subgroup (e.g., by gender) was required, resulting in a total sample of 128 images (256 sides). Convenience sampling was utilized, with consecutive eligible images selected until the target sample size was achieved. No patients were directly recruited, as the study utilized existing anonymized imaging data obtained for routine clinical indications such as implant planning or orthodontic assessment.

Imaging Protocol

CBCT scans were acquired using two calibrated devices to reflect real-world clinical variability while maintaining diagnostic quality. Scans were performed with either the VILLA-ROTOGRAPH EVO system (Villa Sistemi Medicali, Italy; field of view [FOV] 8.5 × 8.5 cm, voxel resolution 0.185 mm, tube voltage 80-90 kVp, tube current 5-10 mA, exposure time 15-20 seconds) or the Kodak CS 9300 system (Carestream Health, France; FOV 10 × 10 cm, voxel size 0.18 mm, tube voltage 85 kVp, tube current 8 mA, exposure time 12 seconds). All acquisitions followed the manufacturer's recommended protocols for maxillofacial imaging, with patients positioned upright and the occlusal plane parallel to the floor to minimize artifacts.

Images were exported in Digital Imaging and Communications in Medicine (DICOM) format and viewed using OnDemand3D software (Cybermed Inc., Seoul, South Korea), which allowed multiplanar reconstructions (axial, coronal, sagittal, and parasagittal) with adjustable slice thickness (0.2-0.5 mm) and contrast enhancement for optimal visualization of bony structures.

Morphological Evaluation

All images were independently evaluated by two trained observers: a board-certified maxillofacial radiologist with over 10 years of experience in CBCT interpretation and a final-year dental student under supervision. Evaluations were conducted on high-resolution monitors (1920 × 1080 pixels) in a dimly lit room to reduce glare and enhance detail perception. Multiplanar views were utilized to trace the IOC from the inferior orbital fissure to the IOF, with axial and parasagittal planes primarily used for classification to assess nerve protrusion relative to the maxillary sinus roof.

IOC morphologies were classified into four types based on the degree of protrusion of the infraorbital nerve from the maxillary roof into the sinus lumen, as described by Acar et al. (2018):

- Type 1: The canal is entirely embedded within the bony roof of the maxillary sinus, with no protrusion (Illustrated in Fig. 1A and 1B).
- Type 2: The canal partially protrudes into the maxillary sinus lumen while remaining attached to the roof (Illustrated in Fig. 1C and 1D).
- Type 3: The canal fully protrudes into the sinus lumen, suspended and attached only by a bony base or septum (Illustrated in Fig. 1E and 1F).
- Type 4: The canal is located laterally, within the zygomatic recess of the maxilla (lateroantral position), without sinus protrusion (Illustrated in Fig. 1G and 1H).

Figure 1. Multiplanar cone-beam computed tomography (CBCT) views demonstrating the four morphological types of the infraorbital canal (IOC) according to the classification of Acar et al.

(A) Axial view showing Type 1 IOC on the right side (canal completely embedded within the bony roof of the maxillary sinus with no protrusion) and Type 2 IOC on the left side (partial protrusion into the sinus lumen while remaining attached to the roof).
(B) Parasagittal view of the right side confirming Type 1 morphology, with the canal fully contained within the bony roof.
(C) Axial view of bilateral Type 2 IOC (partial protrusion into the maxillary sinus).
(D) Parasagittal view illustrating Type 2 morphology.
(E) Axial view of bilateral Type 3 IOC (complete protrusion/suspension of the canal into the sinus lumen).
(F) Parasagittal view of Type 3 IOC on the right side.
(G) Coronal view of bilateral Type 4 IOC (lateroantral position within the zygomatic recess of the maxilla).
(H) Axial view showing the lateral course of Type 4 IOC, with the infraorbital foramen visible at the anterior end of the nerve.

(Classification adapted from Acar et al., 2018; scale bar = 1 cm) (6).

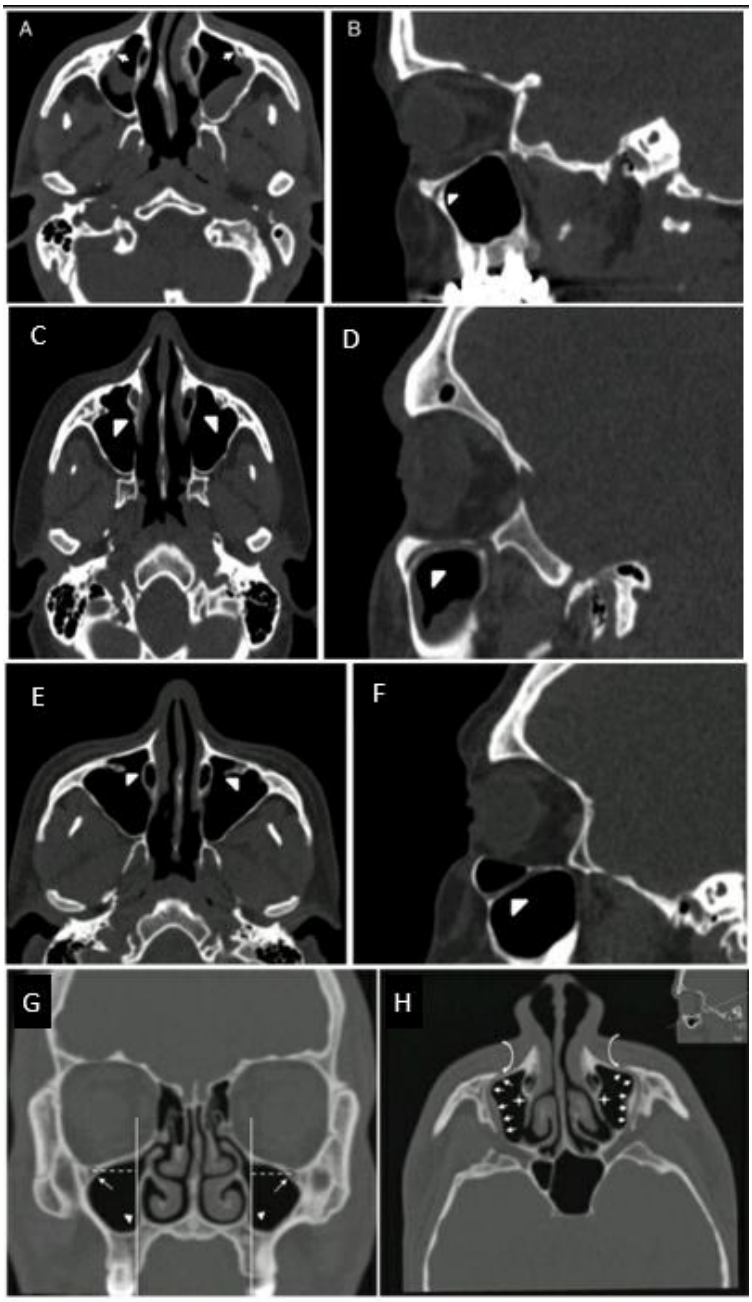

A
B
C
D
E
F
G
H

Figure 2. Multiplanar cone-beam computed tomography (CBCT) illustrations of the four morphological types of the infraorbital canal (IOC) in coronal and parasagittal views.

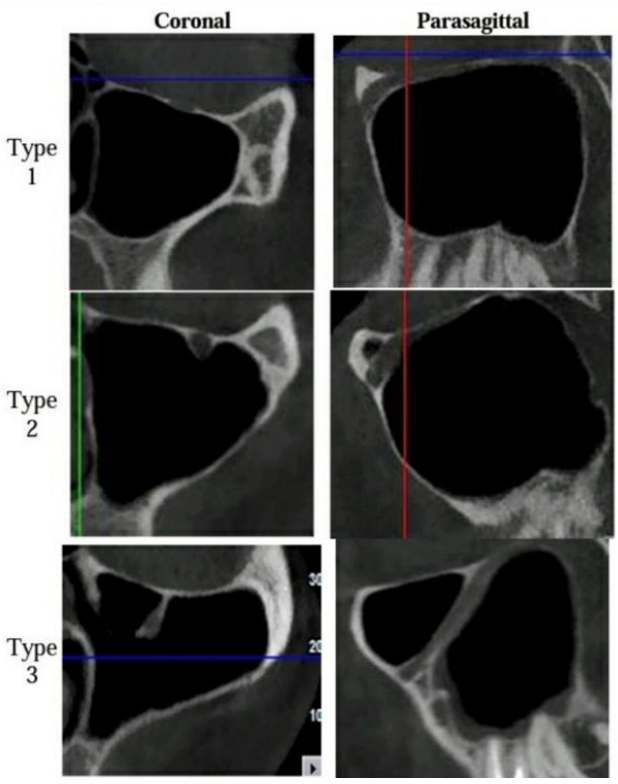
(A) Type 1: Canal completely embedded within the bony roof of the maxillary sinus.

(B) Type 2: Partial protrusion of the canal into the sinus lumen while remaining attached to the roof.

(C) Type 3: Complete protrusion (suspension) of the canal into the maxillary sinus lumen.

(D) Type 4: Lateroantral position of the canal within the zygomatic recess.

(figure adapted from Haghnegahdar et al., 2018; scale bar = 1 cm) (11).



IOF shapes were categorized into three groups based on their outline in coronal and axial reconstructions:

- Oval: Elongated elliptical contour.
- Triangular: Three-sided angular contour.
- Semilunar/circular: Curved or rounded contour.

This categorization followed established morphometric approaches in CBCT studies. Additional variables recorded included patient age (continuous and dichotomized as <30 years and ≥30 years for subgroup analysis, based on the sample median), gender (male/female), side (left/right), and bilateral symmetry. Discrepancies between observers were resolved by consensus discussion; no formal kappa statistic was

calculated due to the retrospective nature and high initial agreement (>95%), but this method ensured reliability consistent with similar radiological studies.

Statistical Analysis

Data were entered into a standardized form and analyzed using IBM SPSS Statistics version 26.0 (IBM Corp., Armonk, NY, USA). Bar charts were generated for descriptive visualization of categorical variables by gender, side, age group, and symmetry. Descriptive statistics were computed, including frequencies and percentages for categorical variables (e.g., IOC types, IOF shapes) and means with SDs for continuous variables (e.g., age). Normality of distributions was assessed using the Kolmogorov-Smirnov test. Chi-square tests (or Fisher's exact test for expected cell counts <5) were employed to compare frequencies of IOC types and IOF shapes across genders, sides, age groups, and symmetry statuses. Analysis of variance (ANOVA) was used for any quantitative morphometric comparisons if applicable, though the primary focus was qualitative classification. All tests were two-tailed, with statistical significance set at $P < 0.05$. No adjustments for multiple comparisons were made, as analyses were exploratory.

Results

The final dataset comprised CBCT images from 128 patients (64 females [50.0%] and 64 males [50.0%]; mean age, 30.45 ± 12.6 years; range, 14-77 years). All images met inclusion criteria, providing bilateral assessments for a total of 256 IOCs and IOFs. No images were excluded post-selection, and observer consensus was achieved for all classifications without major discrepancies.

Infraorbital Foramen (IOF) Morphology

The distribution of IOF shapes across the 256 foramina revealed a predominant oval morphology in 218 cases (85.2%), followed by circular in 29 cases (11.3%) and triangular in 9 cases (3.5%). Stratification by gender showed similar patterns: among females (128 sides), oval shapes accounted for 110 (85.9%), circular for 13 (10.2%), and triangular for 5 (3.9%); among males (128 sides), oval shapes were observed in 108 (84.4%), circular in 16 (12.5%), and triangular in 4 (3.1%). Chi-square analysis indicated no significant difference in IOF shape distribution between genders ($\chi^2 = 0.935$, $df = 2$, $P = 0.351$).

Analysis by side demonstrated near-identical frequencies: on the right side (n=128), oval shapes predominated in 109 (85.2%), circular in 15 (11.7%), and triangular in 4 (3.1%); on the left side (n=128), oval in 109 (85.2%), circular in 14 (10.9%), and triangular in 5 (3.9%). No significant side-related differences were detected ($\chi^2 = 0.096$, $df = 2$, $P = 0.953$).

Age-stratified analysis, dichotomized at the median age (<30 years: n=64 patients, 128 sides; ≥30 years: n=64 patients, 128 sides), showed comparable distributions. In the younger group, oval shapes were present in 110 (85.9%), circular in 14 (10.9%), and triangular in 4 (3.1%); in the older group, oval in 108 (84.4%), circular in 15 (11.7%), and triangular in 5 (3.9%). Chi-square testing confirmed no significant age-related variation ($\chi^2 = 0.195$, df = 2, P = 0.907).

Bilateral symmetry in IOF shape was observed in 113 patients (88.3%), with asymmetry in 15 (11.7%). Among symmetric cases, oval shapes were most common (n=102, 79.7% of total patients), followed by circular (n=10, 7.8%) and triangular (n=1, 0.8%). The high symmetry rate underscores the bilateral consistency of IOF morphology in this cohort (Table 1, 2).

Symmetry analysis indicated moderate bilateral consistency in IOF shape (88.3% symmetric cases), with oval morphology showing the highest agreement across sides. Bar charts illustrated uniform distributions by gender and age groups, confirming no significant variations (χ^2 tests, P > 0.05 for all subgroups).

Infraorbital Canal (IOC) Morphology

IOC classification across 256 canals identified Type 1 as the most prevalent in 147 cases (57.4%), followed by Type 2 in 74 (28.9%), Type 4 in 25 (9.8%), and Type 3 in 10 (3.9%). Gender-specific breakdowns revealed: in females (128 sides), Type 1 in 76 (59.4%), Type 2 in 35 (27.3%), Type 3 in 5 (3.9%), and Type 4 in 12 (9.4%); in males (128 sides), Type 1 in 71 (55.5%), Type 2 in 39 (30.5%), Type 3 in 5 (3.9%), and Type 4 in 13 (10.2%). Overall, no significant gender difference was found in IOC type distribution ($\chi^2 = 0.725$, df = 3, P = 0.867). However, within-gender comparisons using chi-square goodness-of-fit tests indicated Type 1 predominance in females ($\chi^2 = 10.25$, df = 3, P = 0.0046) and males ($\chi^2 = 11.78$, df = 3, P = 0.0013).

Side-specific analysis showed balanced distributions: on the right (n=128), Type 1 in 74 (57.8%), Type 2 in 37 (28.9%), Type 3 in 5 (3.9%), and Type 4 in 12 (9.4%); on the left (n=128), Type 1 in 73 (57.0%), Type 2 in 37 (28.9%), Type 3 in 5 (3.9%), and Type 4 in 13 (10.2%). No significant side differences emerged ($\chi^2 = 0.048$, df = 3, P = 0.997).

Age-group comparisons mirrored the overall pattern: in the <30 years group (128 sides), Type 1 in 75 (58.6%), Type 2 in 36 (28.1%), Type 3 in 5 (3.9%), and Type 4 in 12 (9.4%); in the ≥30 years group (128 sides), Type 1 in 72 (56.3%), Type 2 in 38 (29.7%), Type 3 in 5 (3.9%), and Type 4 in 13 (10.2%). Chi-square analysis showed no significant age effect ($\chi^2 = 0.187$, df = 3, P = 0.980).

Bilateral symmetry in IOC type was evident in 95 patients (74.2%), with asymmetry in 33 (25.8%). Symmetric cases were led by Type 1 (n=61, 47.7% of total patients), followed by Type 2 (n=22, 17.2%),

Type 4 (n=9, 7.0%), and Type 3 (n=3, 2.3%). The symmetry rate was statistically significant for Type 1 predominance ($\chi^2 = 15.42$, df = 3, $P < 0.0001$) (Table 3, 4).

Symmetry evaluation revealed moderate bilateral alignment in IOC type (74.2% symmetric cases), predominantly for Type 1 (47.7%). Bar charts highlighted consistent patterns across gender, side, and age, with no overall differences but within-gender predominance of Type 1 (χ^2 goodness-of-fit, females P=0.0046; males P=0.0013).

No correlations were observed between IOF shape and IOC type (Spearman's rho = 0.045, P = 0.472), nor were there interactions between variables in multivariate ANOVA models ($P > 0.05$ for all).

Overall inferential analyses (chi-square tests) confirmed no significant differences in morphological frequencies by gender (P=0.867 for IOC types; P=0.351 for IOF shapes) or age groups (P=0.980 for IOC; P=0.907 for IOF), supporting hypothesis equivalence across demographics. Symmetry tests indicated moderate bilateral concordance ($P<0.0001$ for Type 1 predominance).

Discussion

The present study provides a detailed analysis of the morphological variations in the infraorbital foramen (IOF) and infraorbital canal (IOC) using cone-beam computed tomography (CBCT) in an Iranian adult population, revealing a predominance of oval IOF shapes (85.1%) and Type 1 IOC configurations (57.4%), with high bilateral symmetry rates (88.3% for IOF and 74.2% for IOC) with moderate bilateral concordance confirmed by symmetry tests ($P<0.0001$). These findings align with established literature on maxillofacial anatomy, where oval IOF morphology is consistently reported as the most common variant across diverse populations, ranging from 63.5% to 85% in CBCT-based studies (14). For instance, a recent morphometric analysis in pediatric patients with unilateral cleft lip and palate using CBCT demonstrated similar oval predominance (approximately 70-80% on non-cleft sides), though with asymmetries on the affected side, highlighting developmental influences not observed in our non-cleft adult cohort (2). Comparatively, in a published article in 2024 in Indian people ,evaluating IOC and IOF variations in 200 CBCT scans, oval shapes comprised 72.5%, with no significant gender differences (P=0.42), mirroring our results (P=0.351) and suggesting that IOF shape may be less influenced by sexual dimorphism than by ethnic or age-related factors (15). The absence of side-specific differences in IOF shape (P=0.953) in our sample further corroborates bilateral consistency reported in recent systematic reviews, where asymmetry rates are typically below 15% in non-pathological cases (1). However, age stratification in our study showed no significant variation (P=0.907), contrasting with some earlier reports indicating slight increases in circular shapes with advancing age due to bony remodeling, though a recent study on Turkish population in 2025 on maxillary sinus volume effects similarly found no age-related IOF

changes in adults over 30 years (16). This stability underscores the utility of CBCT for reliable preoperative mapping, as IOF variations can impact local anesthesia efficacy and surgical access in procedures like midface lifts or zygomatic implants.

Overview of Key Findings

Regarding IOC morphology, the high prevalence of Type 1 (57.4%) in our cohort, characterized by the canal embedded within the maxillary sinus roof, is consistent with global patterns observed in CBCT analyses, where Type 1 configurations range from 55% to 68.5% (12). A 2024 systematic review of IOC variants synthesized data from over 2,000 CBCT scans, confirming Type 1 as the most frequent (mean 60.2%), followed by Type 2 (25-30%), with protruding types (3 and 4) being rarer (5-15%), akin to our distributions (Type 2: 28.9%, Type 3: 3.9%, Type 4: 9.8%) (1).

Notably, while overall gender differences were absent (P=0.867), within-group analyses revealed Type 1 predominance in both sexes (females: P=0.0046; males: P=0.0013), diverging from a study in 2018, where Type 2 was more common in males (50.3% overall), potentially attributable to sample demographics or the inclusion of Haller cells, which were not assessed here but have been linked to increased protrusion rates (up to 29%) (11). Recent 2025 research exploring maxillary sinus volume's influence on IOC angulation reported similar Type 1 frequencies (58%) in edentulous patients, with gender-specific angulation differences but no morphological shifts, supporting our findings and emphasizing volumetric factors in canal positioning (2). The lack of side (P=0.997) or age (P=0.980) effects in IOC types aligns with a 2024 exploratory CBCT study on IOC-maxillary sinus interrelationships, which found bilateral symmetry in 75-80% of cases, comparable to our 74.2%, and no age correlations in adults, though pediatric data suggest greater variability due to ongoing pneumatization (17). Bilateral symmetry was particularly pronounced for Type 1 (47.7%, P<0.0001), reinforcing observations from a study by Fontolliet et al in 2019, where symmetric Type 1 canals predominated in 68.5% of sides, but with higher protrusion in ethmoid cell presence, a confounder warranting future investigation (12).

Infraorbital Foramen Morphology

Clinically, these morphological insights have profound implications for maxillofacial and orbital surgeries, where unrecognized IOC protrusions (e.g., Type 3) elevate iatrogenic nerve injury risks, potentially leading to paresthesia in 10-27% of sinus lift or endoscopic procedures (4).

Our low Type 3 prevalence (3.9%) is in contrast to a study conducted using CT scan (11.4%) but aligns with recent CBCT findings (9.5%), suggesting population-specific risks that necessitate tailored

preoperative imaging (6, 18). The high symmetry rates facilitate predictable bilateral planning, yet the 25.8% asymmetry in IOC types highlights the need for individualized CBCT assessments to avoid complications like hemorrhage during orbital floor reconstructions (6). Furthermore, the absence of IOF-IOC correlations (P=0.472) implies independent variation mechanisms, possibly influenced by sinus pneumatization as evidenced in a 2025 study linking larger sinus volumes to increased IOC protrusion and angulation changes with age (2). Integrating these with accessory structures like canalis sinuosus, as explored a research by Aryanezhad et al, could enhance diagnostic accuracy, given its proximity to IOC and potential for mimicking pathologies (19). Overall, our results advocate for routine CBCT in high-risk surgeries, aligning with 2024 guidelines emphasizing three-dimensional imaging to mitigate iatrogenic damage and optimize outcomes in implantology and rhinology (20).

Infraorbital Canal Morphology

Despite its strengths, including a balanced gender sample and rigorous exclusion criteria, this study has limitations inherent to retrospective designs, such as potential selection bias from referral-based imaging and the absence of inter-observer reliability metrics (e.g., kappa coefficients), though consensus minimized discrepancies (21). The dichotomized age grouping may have overlooked nuanced maturational effects, and unassessed confounders like Haller cells or sinus septa—linked to 28-29% protrusion increases in prior studies—could influence IOC variants (6). Additionally, the Iranian-specific cohort limits generalizability, as ethnic variations in IOF metrics (e.g., greater midline distances in males) have been noted in comparative analyses (14). Future research should incorporate larger, multi-ethnic samples with quantitative measurements (e.g., canal length, angulation) and advanced imaging protocols to evaluate dynamic factors like sinus volume, potentially using AI-assisted segmentation for enhanced precision (2).

Conclusion

In conclusion, this cross-sectional CBCT analysis of 128 Iranian patients underscores the predominant oval morphology of the infraorbital foramen (85.1%) and Type 1 configuration of the infraorbital canal (57.4%), with notable bilateral symmetry (88.3% and 74.2%, respectively) and no significant variations by side or age, though gender-specific predominance of Type 1 IOC highlights subtle demographic influences. These findings reinforce the critical role of preoperative three-dimensional imaging in maxillofacial and sinus surgeries to mitigate iatrogenic risks to the infraorbital nerve, such as paresthesia or hemorrhage, particularly in populations with ethnic-specific anatomical traits like those observed here. By emphasizing the necessity of CBCT for accurate morphometric assessment, this study contributes to enhanced surgical planning and patient safety, advocating for its routine integration in clinical protocols

while calling for future multicenter investigations to explore confounding factors like Haller cells and sinus volume in diverse cohorts.

Declarations

Ethical Approval and Consent to Participate

This retrospective study utilized anonymized cone-beam computed tomography (CBCT) images originally acquired for routine clinical diagnostic purposes. As per institutional protocol at a dental school, patients provided general informed consent upon admission for the use of their anonymized imaging data in educational and research activities. The study was approved by the Institutional Review Board of a dental school (approval number IR.IAU.DENTAL.REC.1399.306), and additional individual patient consent was waived due to the use of fully de-identified archival data with no risk to participants, in accordance with the Declaration of Helsinki (2013 revision). All data were handled in compliance with local data protection regulations.

Consent for Publication

Not applicable.

Abbreviations

ALARA: As Low As Reasonably Achievable

ANOVA: Analysis of Variance

AIOF: Accessory Infraorbital Foramen

CBCT: Cone-Beam Computed Tomography

CT: Computed Tomography

DICOM: Digital Imaging and Communications in Medicine

FOV: Field of View

IOF: Infraorbital Foramen

IOG: Infraorbital Groove

ION: Infraorbital Nerve

IOC: Infraorbital Canal

kVp: Kilovolt Peak

MS: Maxillary Sinus

mA: Milliampere

SD: Standard Deviation

SPSS: Statistical Package for the Social Sciences

STROBE: Strengthening the Reporting of Observational Studies in Epidemiology

μSv: Microsievert

Availability of Data and Materials

The datasets used and/or analyzed during the current study are available from the corresponding author on reasonable request and subject to institutional data-sharing policies.

Competing Interests

The authors declare that they have no competing interests.

Funding

This research received no external funding. All imaging and software resources were provided through the clinical and academic facilities of a dental school and the collaborating private radiology center.

Authors' Contributions

Author 1 contributed to the study conception, design, imaging assessments, and data interpretation. Author 2 performed data collection and statistical analysis. Author 3 contributed to the preparation of the article in terms of content, translation, and final revision. All authors read and approved the final manuscript.

Author 3 is the corresponding author.

Acknowledgements

The authors express gratitude to the radiology staff participating dental school and the collaborating private maxillofacial radiology center for their support in image retrieval and technical assistance.

Transparency Statement

The authors confirm that all content in this manuscript was developed through their intellectual efforts, with no use of artificial intelligence tools for text generation, ensuring originality and adherence to academic integrity standards

References

1. Orellana-Donoso M, Romero-Zucchino D, Fuentes-Abarca A, Aravena-Ríos P, Sanchis-Gimeno J, Konschake M, et al. Infraorbital canal variants and its clinical and surgical implications. A systematic review. Surg Radiol Anat. 2024;46(7):1027-46.
2. Haylaz E, Kalabalık F, Gumussoy I, Duman SB, Eren MC, Say S, et al. Morphometric Analysis of the Infraorbital Foramen in Children and Adolescents with Unilateral Cleft Lip and Palate: A CBCT Study. Children (Basel). 2025;12(10).
3. Vaezi M, Karagah A, Taghavi-Damghani F, Tofangchiha M, Alizadeh A, Reda R, et al. Morphometric analysis of the infraorbital groove, canal, and foramen on computed tomography scans of an Iranian population. Odovtos - International Journal of Dental Sciences. 2025:160-73.

4. Ference EH, Smith SS, Conley D, Chandra RK. Surgical anatomy and variations of the infraorbital nerve. Laryngoscope. 2015;125(6):1296-300.
5. Misch CE. Contemporary Implant Dentistry: Elsevier Health Sciences; 2007.
6. Açar G, Özen KE, Güler İ, Büyükmumcu M. Computed tomography evaluation of the morphometry and variations of the infraorbital canal relating to endoscopic surgery. Braz J Otorhinolaryngol. 2018;84(6):713-21.
7. Venkatesh E, Elluru SV. Cone beam computed tomography: basics and applications in dentistry. J Istanb Univ Fac Dent. 2017;51(3 Suppl 1):S102-s21.
8. Yesilova E, Bayrakdar IS. The Appearance of The Infraorbital Canal and Infraorbital Ethmoid (Haller's) Cells on Panoramic Radiography of Edentulous Patients. Biomed Res Int. 2018;2018:1293124.
9. Jacobs R, Salmon B, Codari M, Hassan B, Bornstein MM. Cone beam computed tomography in implant dentistry: recommendations for clinical use. BMC Oral Health. 2018;18(1):88.
10. Shukla S, Chug A, Afrashtehfar KI. Role of Cone Beam Computed Tomography in Diagnosis and Treatment Planning in Dentistry: An Update. J Int Soc Prev Community Dent. 2017;7(Suppl 3):S125-s36.
11. Haghnegahdar A, Khojastepour L, Naderi A. Evaluation of Infraorbital Canal in Cone Beam Computed Tomography of Maxillary Sinus. J Dent (Shiraz). 2018;19(1):41-7.
12. Fontolliet M, Bornstein MM, von Arx T. Characteristics and dimensions of the infraorbital canal: a radiographic analysis using cone beam computed tomography (CBCT). Surg Radiol Anat. 2019;41(2):169-79.
13. Suttakul P, Vo D, Fongsamootr T, Wanison R, Mona Y, Katongtung T, et al. The role of machine learning for insight into the material behavior of lattices: A surrogate model based on data from finite element simulation. Results in Engineering. 2024;23:102547.
14. Nanayakkara D, Peiris R, Mannapperuma N, Vadysinghe A. Morphometric Analysis of the Infraorbital Foramen: The Clinical Relevance. Anat Res Int. 2016;2016:7917343.
15. Kaushik R, Rapaka R. AI-driven evolution in teledentistry: A comprehensive overview of technology and clinical applications. Dentistry Review. 2025;5(2):100154.
16. Açar G, Gökşan AS, Magat G. The Effect of the Maxillary Sinus Volume on the Morphology and Angulation of the Infraorbital Canal in Relation to Age and Gender. Aesthetic Plast Surg. 2025;49(7):1823-32.
17. Patil K, Sanjay CJ, Basavarajappa R, Christopher VS, Niranjan S. Anatomical interrelationship between infraorbital canal and maxillary sinus: a CBCT-driven exploratory study. European Journal of Anatomy. 2025;29(1):47-55.
18. Gautam R, Adhikari D, Dhital M, Thakur S, Adhikari B. The Prevalence of Protrusion of Infraorbital Nerve into Maxillary Sinus identified on CT Scan of the Paranasal Sinuses at a Tertiary Hospital in Nepal. Nepalese Journal of Radiology. 2018;8(1):7-12.
19. Aryanezhad SS, Jafari-Pozve N, Abrishami M, Arianezhad SM. Investigating the Anatomy and Location of the Infraorbital Canal in Relation to the Adjacent Structures in Cone Beam Computed Tomography (CBCT) Images. J Maxillofac Oral Surg. 2025;24(2):542-56.
20. Lübbers H-T, Bornstein MM, Dagassan-Berndt D, Filippi A, Suter VGA, Dula K. Revised consensus guidelines for the use of cone-beam computed tomography/ digital volume tomography: Results from a consensus process organized by the Swiss association of dentomaxillofacial radiology. SWISS DENTAL JOURNAL SSO – Science and Clinical Topics. 2025;134(4):86-115.
21. Orhan K, Misirli M, Aksoy S, Hincal USE, Ormeci T, Arslan A. Morphometric Analysis of the Infraorbital Foramen, Canal and Groove Using Cone Beam CT: Considerations for Creating Artificial Organs. The International Journal of Artificial Organs. 2016;39(1):28-36.

Tables:

Table 1. Distribution of Infraorbital Foramen Shapes by Gender

Shape	Females (n=128 sides), n (%)	Males (n=128 sides), n (%)	Total (n=256 sides), n (%)	P-value*
Oval	110 (85.9)	108 (84.4)	218 (85.2)	0.351
Circular	13 (10.2)	16 (12.5)	29 (11.3)	
Triangular	5 (3.9)	4 (3.1)	9 (3.5)	

*P-value from chi-square test.

Table 2. Bilateral Symmetry of Infraorbital Foramen Shapes (n=128 Patients)

Symmetry Status	Oval, n (%)	Circular, n (%)	Triangular, n (%)	Total Symmetric, n (%)
Symmetric	102 (79.7)	10 (7.8)	1 (0.8)	113 (88.3)
Asymmetric	-	-	-	15 (11.7)

Table 3. Distribution of Infraorbital Canal Types by Gender

Type	Females (n=128 sides), n (%)	Males (n=128 sides), n (%)	Total (n=256 sides), n (%)	P-value* (Overall)
1	76 (59.4)	71 (55.5)	147 (57.4)	0.867
2	35 (27.3)	39 (30.5)	74 (28.9)	
3	5 (3.9)	5 (3.9)	10 (3.9)	
4	12 (9.4)	13 (10.2)	25 (9.8)	

*P-value from chi-square test. Within-group P-values: females, P=0.0046; males, P=0.0013 (goodness-of-fit).

Table 4. Bilateral Symmetry of Infraorbital Canal Types (n=128 Patients)

Symmetry Status	Type 1, n (%)	Type 2, n (%)	Type 3, n (%)	Type 4, n (%)	Total Symmetric, n (%)
Symmetric	61 (47.7)	22 (17.2)	3 (2.3)	9 (7.0)	95 (74.2)
Asymmetric	-	-	-	-	33 (25.8)

$P<0.0001$ for Type 1 predominance (chi-square goodness-of-fit).